Available online at www.sciencedirect.com
ScienceDirect
Journal of Sound and Vibration 322 (2009) 969–986
JOURNAL OF SOUND AND VIBRATION
www.elsevier.com/locate/jsvi

A large deflection model for the pull-in analysis of electrostatically actuated microcantilever beams

S. Chaterjee, G. Pohit*

Department of Mechanical Engineering, Jadavpur University, Kolkata 700032, India

Received 7 August 2008; received in revised form 4 October 2008; accepted 15 November 2008
Handling Editor: L.G. Tham
Available online 19 January 2009

Abstract

A comprehensive model of an electrostatically actuated microcantilever beam separated from the ground plane by relatively larger gap is formulated accounting for the nonlinearities of the system arising out of electric forces, geometry of the deflected beam and the inertial terms. Since the gap is relatively large, the electrostatic model is formulated incorporating higher order correction of electrostatic forces. First static analysis is carried out to match the results obtained from the proposed model with the results provided by other researchers. It is observed that reduced order model exhibits good convergence when five or more number of modes is considered for the analysis. Dynamic analysis of the model is performed with five modes. The study indicates that although electrostatic forces cause softening characteristics whereas geometric nonlinearity produces stiffening effect on the microstructure, the nonlinearities play a significant role when pull-in occurs. The consideration of slope and curvature of deformable electrode for modelling the electrostatic forces for large gap separations predicts more accurate results. For applications in and around pull-in zone, the large deflection model needs to be considered for effective design.

1. Introduction

Electrostatically actuated devices form a broad class of MEMS devices due to their simplicity, as they require few mechanical components and small voltage levels for actuation [1]. Typical MEMS structures consist of thin beams with cross-sections in the order of microns and lengths in the order of ten to hundreds of microns. Efficient electrostatic actuation at reasonable actuation voltages is achieved for the size of the devices such that the electrostatic gap to beam length is typically of the order of 10^{-2}–10^{-3}. Further reduction in size of the devices, and, low actuation voltages operations have been made possible by the development of new materials and advancement in fabrication technologies. In such devices, the length of the electrode is typically of the order of several micrometers with the gap-length ratio not necessarily small and can be typically of the order of 10^{-1}–10^{-2} [2,3] or even larger [4]. For small gap-length ratios, parallel plate approximation of the electrostatic forces and small deflection assumption for deriving the mechanical model are justified. However,

*Corresponding author. Tel./fax: +91 33 2414 6890.
E-mail address: gpohit@vsnl.net (G. Pohit).

0022-460X/$ - see front matter © 2009 Elsevier Ltd. All rights reserved.
doi:10.1016/j.jsv.2008.11.046

for relatively larger gaps, a model involving geometric nonlinearity and a more accurate approximation of the electrostatic forces needs to be derived. Electrostatically actuated microbeams (e.g., cantilever and fixed–fixed microbeams) are used in many MEMS devices such as capacitive MEMS switches and resonant sensors. Microfabricated cantilever beams are widely used in MEMS capacitive type sensors as the sensing element [5–8]. In case of an electrostatically actuated microcantilever, when the applied voltage is increased beyond a critical value, stable equilibrium positions of the beam cease to exist and the elastic beam is pull-in into the ground plate. This phenomenon known as static pull-in instability has as well been observed experimentally in Refs. [9,10,19]. In case of applications like microswitches [11,12] or micromirror positioning the transient behaviour is of great interest. With voltages applied as non-smooth function of time, the kinetic energy and the dissipation of energy play an important role in defining the dynamic pull-in condition.

The static pull-in voltage depends on the interaction of the nonlinear electrostatic forces and the structural stiffness of the microcantilever. A further complication arises due to redistribution of electrostatic forces owing to deformation of the structure thereby modifying the mechanical restoring forces. As a result, couple field solutions are required. Several approaches have been proposed for the estimation of the static pull-in parameters. From simple lumped models [10,13,14], on one hand, to powerful 3-D numerical simulations [15–17] based on FEM/BEM schemes, on the other hand, have been established to elucidate the pull-in behaviour. The model in Ref. [10] leads to a simplified expression for the pull-in voltage and is not usable for real MEMS structure. A closed form expression for the pull-in voltage has been derived by Pamidighantam et al. [13]. Though membrane stiffness due to large deflection has been considered for clamped–clamped beam, the effective stiffness for cantilever case is valid only for small deflections. The approach of Chowdhury et al. [14] is based on a linearized uniform approximate model of the nonlinear electrostatic pressure and the load deflection model of a cantilever beam under uniform pressure incorporating fringing field corrections. They introduced a compensation factor to compensate for the errors arising out of non-inclusion of the geometric nonlinearity and the linearization of the electrostatic forces. Computer aided design systems MEMCAD was developed [15] to simulate electrostatic MEMS. An automated procedure to generate macromodel from a 3-D FEM simulation was presented in Ref. [16]. This procedure may not be suitable for problems involving large displacements as the mid-plane stretching effect for the clamped–clamped beams was neglected. Coventor [17] provides a comparison of the pull-in voltage results obtained from the COVENTORWARE (FEA) and the ARCHITECT parametric analysis models for various device parameters. FCM, a meshless technique, was used by Gang and Aluru [18] to simulate linear and nonlinear static behaviour in electrostatic MEMS. Effect of different geometric variables on the static pull-in voltage was presented for both clamped–clamped and cantilever beams. Pull-in voltage results obtained through experimental measurements by Hu et al. [19] were compared to the analytical model based on small deflection and linearized electrostatic forces. Nayfeh et al. [20] emphasized the efficacy of accounting for the mid-plane stretching of the beam in order to treat large deflections for clamped–clamped beams. The model successfully highlights the importance of including the deflection distribution, geometric nonlinearities and mid-plane stretching in the analysis to avoid underestimation of the stability limits. Generalized DQM has been used by Osterberg et al. [21] to study the pull-in behaviour of both clamped–clamped and cantilever based MEMS switches. Various effects like fringing field, stress gradient and trapezoidal cross-section were considered.

In addition to the stability of equilibria, transient behaviour of microstructures has also been studied by several authors [11,12,22–28]. Behaviour of cantilever microswitches under step voltages was analysed by McCarthy et al. [11] using finite difference method. The microswitch modelled as a clamped–clamped microbeam actuated by step input was studied by Xie et al. [12] using invariant manifold approach. Full-Lagrangian based relaxation and Newton schemes for dynamic analysis of electrostatic MEMS was presented by Aluru et al. [22]. Static and dynamic pull-in conditions were analytically examined in Ref. [23] using energy analysis of a lumped parameter model. Under dynamic conditions, reduction in stable voltages was obtained whereas the travel range was much extended. Lumped parameter models were used by Nielson et al. [24] for analytical and numerical analyses of both parallel-plate and torsional actuators. For the ideal case of no damping, significant decrease in the pull-in voltage was obtained for an applied step voltage. FEM approach was used [25] to simulate the dynamic behaviour of a clamped–clamped beam type resonator under a suddenly applied voltage. It was shown that the system may become unstable before the static pull-in voltage due to the dynamical effects.

A reduced order model (ROM) was developed by Younis et al. [26] to investigate both static and dynamic pull-in behaviour of a clamped–clamped beam based microdevice. The macromodel uses few linear-undamped mode shapes of a microbeam in its straight position as basis functions in a Galerkin procedure. The model accounts for the mid-plane stretching and the electrostatic force is represented exactly in the discretization procedure. They observed that numerical results obtained using even number of modes did not converge. Using five modes for discretization, pull-in time of a pressure sensor was validated with the experimental results. An elastic cantilever coupled to a plate at the free end was studied by Krylov and Maimon [27] to investigate the static and transient behaviour in the presence of squeeze film damping. A ROM, with three modes used in the discretization procedure, predicted the transient dynamics revealing good agreement with the experimental data. The Lyapunov exponents had been used by Krylov [28] to indicate dynamic pull-in instability of double clamped microbeam actuated by a suddenly applied voltage subjected to nonlinear squeeze film damping. Static analysis results obtained with the ROM were compared with the numeric solution of the boundary value problem (BVP). The number of modes to be used in the discretization procedure was shown to be dependent on the nonlinear parameter representing geometric nonlinearity. The transient behaviour obtained with the reduced order and finite difference models were in good agreement for an undamped beam. Batra et al. [29] considered the von Kármán nonlinearity and the Casimir force to first develop a reduced-order model for a prestressed clamped elliptic electrostatically actuated microplate and studied vibrations and pull-in instability of the system. However, the effect of inertia forces on pull-in parameters has not been analysed. Electromechanical Models have been proposed for narrow microbeam and parallel array of microplates under the influence of electric field [30,31]. A closed-form expression was derived in Ref. [31] to study the modal properties and pull-in instability of the array. A study was undertaken in Ref. [32] to determine the exact mode shapes of vibrations that are inevitably required in the study of the system in the time-domain, as well as the stability of electrostatic exciter/detector. An overview of models for electrostatically devices classifying the theoretical, numerical and experimental works according to the mechanical model used in the analyses has been presented in Ref. [33].

In this paper, the static and dynamic pull-in behaviours of wide microcantilevers separated by relatively larger gaps and acted upon by DC electrostatic forces are studied. The structural geometric nonlinearity due to large deformation effect is quite considerable in microstructures because of their low mass and high flexibility. For large gaps between the deformable conductor and the ground plane, slope and curvature of the deformable electrode also needs to be considered for modelling the electrostatic pressure [34]. Few conclusive studies, investigating the effect of geometric and inertial nonlinearities on the response of electrically actuated wide microcantilevers separated by large gaps, exist in the literature. A comprehensive model is derived accounting for the nonlinearities of the system due to electric forces, the geometry of the deflected beam, and the inertial terms. As studied in the earlier works [29–32,35–40] with varying levels of complexity and sophistication, the nonlinear curvature and the von Kármán nonlinearity in the axial strain–displacement relationship are incorporated to account for the geometric nonlinearity of the microcantilever associated with large deflection. The compatibility of the electrostatic model, with the large deflection theory being used for the structural model, has been taken care off by incorporating higher order correction of the electrostatic forces [34]. From the comprehensive model, a ROM is developed to study the effect of nonlinearities on the static response and the transient dynamics. An investigation is carried out in detail to ascertain number of modes to be employed for ROM analysis to arrive at results within admissible error. Efficacy of the large deflection model, for behavioural simulations of electrostatic MEMS, with respect to gap-length ratio of the devices has been demonstrated in this study.

The rest of the paper is organized as follows. In Sections 2 and 3, respectively, the electromechanical model and the related BVP have been described. In Section 4, the ROM has been formulated using Galerkin method. In Section 5, the BVP governing the static deflection has been numerically solved. The results have been validated with the experimental results available in open literature. Further, the ROM with the correct number of modes has been used to simulate the transient dynamics. The dynamic results have been validated with the numerical results available in the literature. Influences of nonlinearities arising out of electrostatic forces, geometry, and the inertial terms are studied. Conclusions are summarized in Section 6.

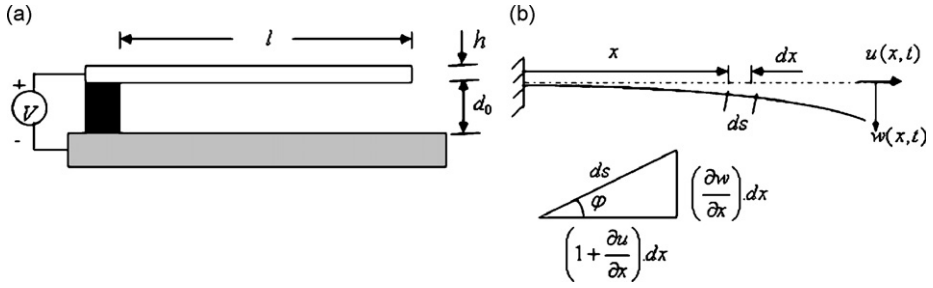

Fig. 1. (a) A schematic diagram of an electrostatically actuated microcantilever beam model and (b) a schematic diagram of a deflected microcantilever beam.

2. Model description

Fig. 1 illustrates a perfect conductor clamped at one end through dielectric support and suspended over a ground plane. The upper electrode is acted upon by attractive electrostatic force which is non-uniformly distributed along the length due to the redistribution of the charges as the beam deflects. Even at small voltages, the tip deflection will be comparable to the air-gap and will be large enough in comparison to the electrode thickness. The deformable electrodes with thickness much smaller than the characteristic in-plane dimension can be treated as 2D plate like bodies [29,31,41]. In this work, the electrostatic force is assumed to be uniform across the width and the deformable conductor is assumed to undergo cylindrical bending deformations and is treated as a wide (width-thickness ratio greater than 5) beam with the effective Young's modulus equal to the plate modulus [20,42]. Under large rigid-body rotations, structures like cantilever beams undergo large deformations but small strains, and the beam can be modelled by incorporating the von Kármán nonlinearity in the expression for the axial strain [29–32] and consideration of nonlinear curvature [35–40]. Fringing fields emanating from the lateral and the top surfaces of the deformable electrode need to be considered while modelling the electrostatic field by accounting for finite width and finite thickness [43,44] of the beam. For wide beams with beamwidth–airgap ratio greater than 1.5 [43] and width-thickness ratio greater than 5 [44], the fringing fields are neglected. For flexible structures, the parallel plate capacitance (PPC) is usually justified by the smallness of the gap-length ratio typically of the order of 10^{-2}–10^{-3} [45]. The present work for relatively larger gaps incorporates the second order corrections (SOC) [34] to formulate the electrostatic model.

3. Boundary value problem (BVP)

The model (Fig. 1) shows an undamped cantilever beam of length l, width b, thickness h separated from the ground plane by an initial gap of d_0. When subjected to a driving DC voltage V, the beam undergoes a transverse deflection $w(x,t)$ and an axial extension $u(x,t)$, which are dependent on the position x along the beam length and time t. Geometric nonlinearity arises from two distinct mechanisms: (1) Green strain relation that quantifies the extensional deformation of the centroidal plane of the beam, and (2) the nonlinear curvature of the deflection curve. The axial strain ξ_{xx} [37] associated with the material located at the neutral axis is given by

$$\xi_{xx} = \frac{\mathrm{d}s - \mathrm{d}x}{\mathrm{d}x} = \left[\left(1 + \frac{\partial u(x,t)}{\partial x}\right)^2 + \left(\frac{\partial w(x,t)}{\partial x}\right)^2\right]^{1/2} - 1 \tag{1}$$

Using the inextensibility condition (i.e., $\xi_{xx} = 0$) in Eq. (1), one gets

$$\left(1 + \frac{\partial u}{\partial x}\right)^2 + \left(\frac{\partial w}{\partial x}\right)^2 = 1 \tag{2}$$

Following [39] and as shown in Fig. 1, the exact expression for the nonlinear curvature k can be given by

$$k = \frac{\partial \varphi}{\partial s} = \frac{\left(1 + \frac{\partial u}{\partial x}\right)\frac{\partial^2 w}{\partial x^2} - \frac{\partial^2 u}{\partial x^2} \cdot \frac{\partial w}{\partial x}}{\left[\left(1 + \frac{\partial u}{\partial x}\right)^2 + \left(\frac{\partial w}{\partial x}\right)^2\right]^{3/2}} \tag{3}$$

Using Eq. (2), one can express Eq. (3) as

$$k = \left(1 + \frac{\partial u}{\partial x}\right)\frac{\partial^2 w}{\partial x^2} - \frac{\partial^2 u}{\partial x^2} \cdot \frac{\partial w}{\partial x} \tag{4}$$

The bending strain energy U_s of the beam is given by

$$U_s = \frac{1}{2}\int_0^l E \cdot I \cdot k^2 \, \mathrm{d}x \tag{5}$$

where plate modulus $E = E'/(1 - v^2)$, E' is the Young's modulus, v is the Poisson's ratio. The beam is assumed to be prismatic with rectangular cross section, thereby the moment of inertia and the area of the cross section can be given by $I = bh^3/12$ and $A = bh$, respectively. The kinetic energy T of the beam can be expressed as

$$T = \frac{1}{2}\int_0^l \rho A\left(\frac{\partial w}{\partial t}\right)^2 \mathrm{d}x + \frac{1}{2}\int_0^l \rho A\left(\frac{\partial u}{\partial t}\right)^2 \mathrm{d}x \tag{6}$$

where ρ is the density of the beam material.

Neglecting fringing field capacitance due to width, due to thickness, and, at the free end of the cantilever, and following [34], the electrical potential energy U_e stored between the beam and the ground plane for large gap separation is given by

$$U_e = -\frac{1}{2}\varepsilon_0 b V^2 \int_0^l \frac{1}{(d_0 - w)}\left[1 + \frac{(d_0/l)^2}{3} \cdot \frac{1}{d_0^2} \cdot \left\{\frac{\partial}{\partial x}(d_0 - w)\right\}^2\right]\mathrm{d}x \tag{7}$$

where permittivity constant for free space, $\varepsilon_0 = 8.854 \times 10^{-12}\ \mathrm{F\,m^{-1}}$. It may be noted that Eq. (7) incorporates the corrections up to the second order.

Using Eqs. (4)–(7), and retaining all nonlinearities up to $O(\varepsilon^3)$, where $x/l = O(1)$, $w/l = O(\varepsilon)$, and $u/l = O(\varepsilon^2)$, the set of governing equations of motion of the system using Hamilton principle can be obtained as

$$\begin{aligned}\rho A\frac{\partial^2 w}{\partial t^2} + EI\frac{\partial^2}{\partial x^2}\left[\frac{\partial^2 w}{\partial x^2} + 2\frac{\partial^2 w}{\partial x^2}\frac{\partial u}{\partial x} - \frac{\partial^2 u}{\partial x^2}\frac{\partial w}{\partial x}\right] + EI\frac{\partial}{\partial x}\left[\frac{\partial^2 w}{\partial x^2}\frac{\partial^2 u}{\partial x^2}\right] \\ = \frac{1}{2}\frac{\varepsilon_0 b V^2}{(d_0 - w)^2}\left[1 - \frac{(d_0/l)^2}{3d_0^2}\left\{\left(\frac{\partial w}{\partial x}\right)^2 + 2(d_0 - w)\frac{\partial^2 w}{\partial x^2}\right\}\right]\end{aligned}$$

and

$$-\rho A\frac{\partial^2 u}{\partial t^2} + EI\frac{\partial^2}{\partial x^2}\left[\frac{\partial^2 w}{\partial x^2}\frac{\partial w}{\partial x}\right] + EI\frac{\partial}{\partial x}\left[\left(\frac{\partial^2 w}{\partial x^2}\right)^2\right] = 0 \tag{8}$$

Using Eq. (2) while retaining terms up to $O(\varepsilon^3)$, variable u can be coupled to w. Hence, the equation of motion of the system reduces to its final form as

$$\begin{aligned}&\rho A\frac{\partial^2 w}{\partial t^2} + EI\frac{\partial^4 w}{\partial x^4} + EI\frac{\partial}{\partial x}\left[\frac{\partial w}{\partial x}\frac{\partial}{\partial x}\left(\frac{\partial w}{\partial x} \cdot \frac{\partial^2 w}{\partial x^2}\right)\right] + \rho A\frac{\partial}{\partial x}\left[\frac{\partial w}{\partial x}\int_l^x \int_0^x \left\{\frac{\partial}{\partial x}\left(\frac{\partial^2 w}{\partial t^2}\right)\frac{\partial w}{\partial x} + \left(\frac{\partial}{\partial x}\left(\frac{\partial w}{\partial t}\right)\right)^2\right\}\mathrm{d}x\,\mathrm{d}x\right] \\ &= \frac{1}{2}\frac{\varepsilon_0 b V^2}{(d_0 - w)^2}\left[1 - \frac{(d_0/l)^2}{3d_0^2}\left\{\left(\frac{\partial w}{\partial x}\right)^2 + 2(d_0 - w)\frac{\partial^2 w}{\partial x^2}\right\}\right]\end{aligned} \tag{9a}$$

with the boundary conditions as

$$w(0) = \left.\frac{\partial w}{\partial x}\right|_{x=0} = 0$$

$$\left.\frac{\partial^2 w}{\partial x^2}\right|_{x=l} = \left.\frac{\partial^3 w}{\partial x^3}\right|_{x=l} = 0 \tag{9b}$$

Using the non-dimensional variables $\hat{w} = (w/d_0)$, $\hat{x} = (x/l)$, $\hat{t} = (t/l^2)\sqrt{EI/\rho A}$ the above equation can be expressed as

$$\ddot{w} + w^{iv} + \alpha_1[w'(w'w'')']' + \alpha_1\left[w'\int_1^x\int_0^x \{\ddot{w}'w' + (\dot{w}')^2\}\,dx\,dx\right]' = \frac{\alpha_2}{(1-w)^2}\left[1 - \frac{\alpha_1}{3}\{2w'' - 2ww'' + (w')^2\}\right] \tag{10a}$$

$$w(0,t) = w'(0,t) = 0$$

$$w''(1,t) = w'''(1,t) = 0 \tag{10b}$$

where

$$\alpha_1 = \left(\frac{d_0}{l}\right)^2, \quad \alpha_2 = \frac{6\varepsilon_0 l^4 V^2}{Eh^3 d_0^3}$$

It may be mentioned that over prime and over dot indicates derivative with respect to non-dimensional position and time, respectively. It is to be further noted that caps (^) are removed for convenience. The effect of different design parameters are indicated by Eq. (10a) through the non-dimensional parameters α_1 and α_2. The nonlinear curvature which enters the equation as a cubic term and represented by the third term on the left hand side of the equation, has a stiffening effect on the system. Further, the influence of the nonlinear curvature is dependent on the ratio (α_1) of the initial air-gap distance d_0 to the microbeam length l rather than on their actual values. The influence becomes more prominent as the ratio increases and the results are dictated by the relative values of α_1 and α_2. The SOC of the electrostatic forces which is represented by the second term on the right hand side of the equation depends on the slope and curvature of the deformable beam.

4. Galerkin formulation

Modal decomposition [26] is performed in this section to facilitate the study of transient behaviour of the microcantilever in response to the DC forcing. The method of Galerkin decomposition is employed to approximate the system equations (10) by a ROM composed of a finite number of discrete modal equations. The process of Galerkin decomposition starts with separating the dependences of the deflection of the deformed beam, $w(x,t)$, into temporals and spatials by functions $\sigma_i(t)$ and $\phi_i(x)$, respectively, in the form of a series of products, i.e.,

$$w(x,t) = \sum_{i=1}^{N} \sigma_i(t)\phi_i(x) \tag{11}$$

where N represents the number of modes retained in the solution.

$\phi_i(x)$ is the ith linear undamped mode shape of the undeflected microcantilever obtained from the following linear undamped eigenvalue problem of a straight beam

$$\phi_i^{iv} = \omega_i^2\phi_i \tag{12a}$$

$$\phi_i(0) = \phi_i'(0) = \phi_i''(1) = \phi_i'''(1) = 0 \tag{12b}$$

It is worth mentioning that $\phi_i(x)$ is normalized such that $\int_0^1 \phi_i^2\,dx = 1$.

Multiplying Eq. (10a) by $(1-w)^2$, substituting Eqs. (11) and (12a) into the resulting equation, multiplying by $\phi_n(x)$, and integrating the outcome from $x = 0$ to 1, the coupled nonlinear ODEs of the system can be

derived as

$$\ddot{\sigma}_n + \sigma_n\omega_n^2 + \sum_{i=1}^{N}\sum_{j=1}^{N}\sum_{k=1}^{N}\ddot{\sigma}_i\sigma_j\sigma_k\int_0^1 \phi_n\phi_i\phi_j\phi_k\,\mathrm{d}x - 2\sum_{i=1}^{N}\sum_{j=1}^{N}\ddot{\sigma}_i\sigma_j\int_0^1 \phi_n\phi_i\phi_j\,\mathrm{d}x + \sum_{i=1}^{N}\sum_{j=1}^{N}\sum_{k=1}^{N}\sigma_i\sigma_j\sigma_k\omega_i^2\int_0^1 \phi_n\phi_i\phi_j\phi_k\,\mathrm{d}x$$
$$- 2\sum_{i=1}^{N}\sum_{j=1}^{N}\sigma_i\sigma_j\omega_i^2\int_0^1 \phi_n\phi_i\phi_j\,\mathrm{d}x + \alpha_1\left[\sum_{i=1}^{N}\sum_{j=1}^{N}\sum_{k=1}^{N}\sigma_i\sigma_j\sigma_k\int_0^1 \phi_n\phi_i''\phi_j''\phi_k''\,\mathrm{d}x\right.$$
$$+ \sum_{i=1}^{N}\sum_{j=1}^{N}\sum_{k=1}^{N}\sum_{p=1}^{N}\sum_{q=1}^{N}\sigma_i\sigma_j\sigma_k\sigma_p\sigma_q\int_0^1 \phi_n\phi_i''\phi_j''\phi_k''\phi_p\phi_q\,\mathrm{d}x - 2\sum_{i=1}^{N}\sum_{j=1}^{N}\sum_{k=1}^{N}\sum_{p=1}^{N}\sigma_i\sigma_j\sigma_k\sigma_p\int_0^1 \phi_n\phi_i''\phi_j''\phi_k''\phi_p\,\mathrm{d}x$$
$$+ 4\sum_{i=1}^{N}\sum_{j=1}^{N}\sum_{k=1}^{N}\sigma_i\sigma_j\sigma_k\int_0^1 \phi_n\phi_i'\phi_j''\phi_k''\,\mathrm{d}x + 4\sum_{i=1}^{N}\sum_{j=1}^{N}\sum_{k=1}^{N}\sum_{p=1}^{N}\sum_{q=1}^{N}\sigma_i\sigma_j\sigma_k\sigma_p\sigma_q\int_0^1 \phi_n\phi_i'\phi_j''\phi_k'''\phi_p\phi_q\,\mathrm{d}x$$
$$- 8\sum_{i=1}^{N}\sum_{j=1}^{N}\sum_{k=1}^{N}\sum_{p=1}^{N}\sigma_i\sigma_j\sigma_k\sigma_p\int_0^1 \phi_n\phi_i'\phi_j''\phi_k'''\phi_p\,\mathrm{d}x + \sum_{i=1}^{N}\sum_{j=1}^{N}\sum_{k=1}^{N}\sigma_i\sigma_j\sigma_k\omega_i^2\int_0^1 \phi_n\phi_i\phi'_j\phi_k'\,\mathrm{d}x$$
$$+ \sum_{i=1}^{N}\sum_{j=1}^{N}\sum_{k=1}^{N}\sum_{p=1}^{N}\sum_{q=1}^{N}\sigma_i\sigma_j\sigma_k\sigma_p\sigma_q\omega_i^2\int_0^1 \phi_n\phi_i\phi_j'\phi_k'\phi_p\phi_q\,\mathrm{d}x - 2\sum_{i=1}^{N}\sum_{j=1}^{N}\sum_{k=1}^{N}\sum_{p=1}^{N}\sigma_i\sigma_j\sigma_k\sigma_p\omega_i^2\int_0^1 \phi_n\phi_i\phi_j'\phi_k'\phi_p\,\mathrm{d}x$$
$$+ \sum_{i=1}^{N}\sum_{j=1}^{N}\sum_{k=1}^{N}\ddot{\sigma}_i\sigma_j\sigma_k\int_0^1 \phi_n\beta_{ijk}\,\mathrm{d}x + \sum_{i=1}^{N}\sum_{j=1}^{N}\sum_{k=1}^{N}\sum_{p=1}^{N}\sum_{q=1}^{N}\ddot{\sigma}_i\sigma_j\sigma_k\sigma_p\sigma_q\int_0^1 \phi_n\phi_p\phi_q\beta_{ijk}\,\mathrm{d}x$$
$$- 2\sum_{i=1}^{N}\sum_{j=1}^{N}\sum_{k=1}^{N}\sum_{p=1}^{N}\ddot{\sigma}_i\sigma_j\sigma_k\sigma_p\int_0^1 \phi_n\phi_p\beta_{ijk}\,\mathrm{d}x + \sum_{i=1}^{N}\sum_{j=1}^{N}\sum_{k=1}^{N}\dot{\sigma}_i\dot{\sigma}_j\sigma_k\int_0^1 \phi_n\beta_{ijk}\,\mathrm{d}x$$
$$\left.+ \sum_{i=1}^{N}\sum_{j=1}^{N}\sum_{k=1}^{N}\sum_{p=1}^{N}\sum_{q=1}^{N}\dot{\sigma}_i\dot{\sigma}_j\sigma_k\sigma_p\sigma_q\int_0^1 \phi_n\phi_p\phi_q\beta_{ijk}\,\mathrm{d}x - 2\sum_{i=1}^{N}\sum_{j=1}^{N}\sum_{k=1}^{N}\sum_{p=1}^{N}\dot{\sigma}_i\dot{\sigma}_j\sigma_k\sigma_p\int_0^1 \phi_n\phi_p\beta_{ijk}\,\mathrm{d}x\right]$$
$$- \alpha_2\left[\int_0^1 \phi_n\,\mathrm{d}x - \frac{\alpha_1}{3}\left(2\sum_{i=1}^{N}\sigma_i\int_0^1 \phi_n\phi_i''\,\mathrm{d}x - 2\sum_{i=1}^{N}\sum_{j=1}^{N}\sigma_i\sigma_j\int_0^1 \phi_n\phi_i\phi_j''\,\mathrm{d}x + \sum_{i=1}^{N}\sum_{j=1}^{N}\sigma_i\sigma_j\int_0^1 \phi_n\phi_i'\phi_j'\,\mathrm{d}x\right)\right]$$
$$= 0, \quad n = 1, 2, \ldots, N \tag{13}$$

where $\beta_{ijk} = [\phi_k' \int_1^x \int_0^x \phi_i'\phi_j'\,\mathrm{d}x\,\mathrm{d}x]'$.

It should be noted that the above method of treating the electrostatic force term ensures its exact representation. In the process, the mass matrix of Eq. (13) no longer remains diagonal as obtained in Refs. [27,28].

5. Results

In this section, firstly, the static analysis is carried out by directly solving the BVP. The model is validated for the static pull-in voltage and the static pull-in deflection. The convergence of the model obtained through Galerkin decomposition method is then studied by comparing the results with the static solution of the BVP. The ROM with the correct number of modes is then used to study the dynamic behaviour under an applied voltage varying as non-smooth function of time.

5.1. Static analysis

The static deflection equation is obtained by setting all time derivatives in Eq. (10a) to zero. The two-point BVP was numerically solved for $w(x)$ using the Matlab BVP solver [46]. The numerical procedure implements a collocation method for the solution of two point BVP. The first step is to express the governing equation as a system of first order differential equations (collocates). An initial guess is supplied for each variable used to define the first order differential equations. The guess for an initial mesh is then used by the finite difference code to obtain accurate numerical solution within an absolute tolerance of 10^{-6}. Fig. 2 reveals the existence of two solutions for each value of the gradually applied DC voltage. The pull-in condition is predicted as both the solutions coalesce at a certain voltage. It has been shown by earlier authors [20,28] that the upper-branch solution is unstable whereas the lower branch corresponds to the stable equilibrium configurations. Hereafter,

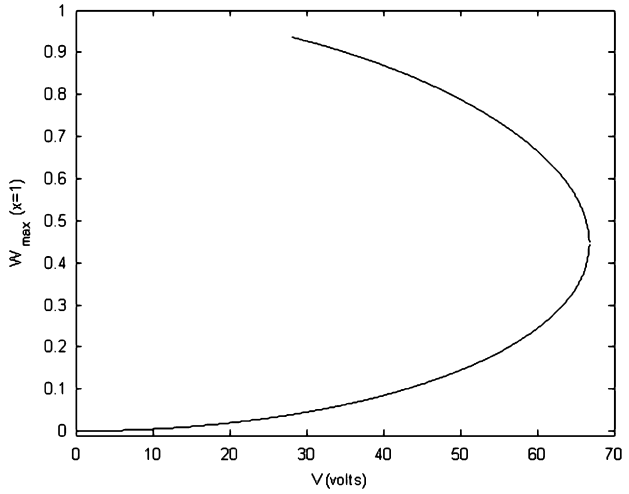

Fig. 2. Variation of the non-dimensional tip deflection w_{max} with voltage V for the beam properties $E' = 155.8e9\,Pa$, $b = 5000e-6\,m$, $h = 57e-6\,m$, $d_0 = 92e-6\,m$, $l = 20000e-6\,m$, $v = 0.06$ as used in Ref. [19].

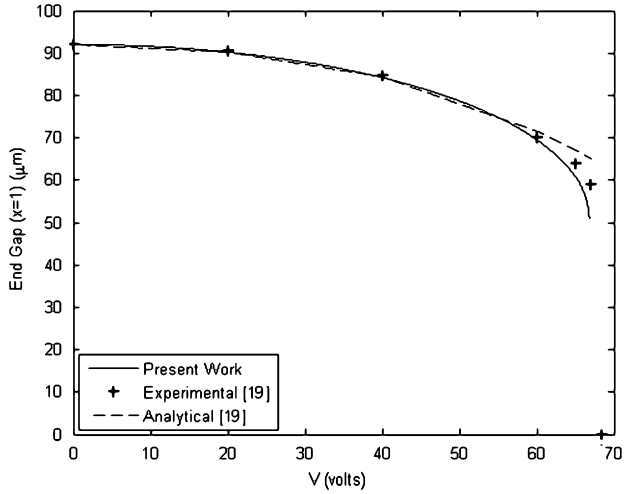

Fig. 3. Comparison of end gap results for $\alpha_1 = 2.1e-5$.

in this paper, the lower branch will suffice for the static deflection of the microcantilever. To validate the proposed model the pull-in results are compared with the results obtained in Ref. [19]. Fig. 3 clearly shows that the pull-in results of the present work are in better agreement with the experimental results in comparison to the analytical results of [19] which are based on linearized electrostatic forces. The estimated static pull-in voltage (V_{SPI}) is 66.78 V using the proposed model compared to 68.5 V obtained experimentally in Ref. [19]. The pull-in voltage predicted in Ref. [21] for the same system configuration was 66.4 V, only after due consideration of fringing field and stress gradient effects which have been neglected in this study.

To study the influence of the nonlinear curvature, the microbeam static deflection equation was solved for a range of electrostatic forces ranging from zero to the forcing level where structural instability (pull-in) develops. This procedure was repeated for various values of α_1. Fig. 4 shows the variation of the non-dimensional tip deflection w_{max} with α_2 for various values of α_1. At low levels of the electrostatic force, represented by α_2, the curve is linear but nonlinearity starts showing its effects as α_2 increases to higher (>1) values. As α_1 increases, the value of α_2 at which pull-in develops also increases. This is in support of the fact

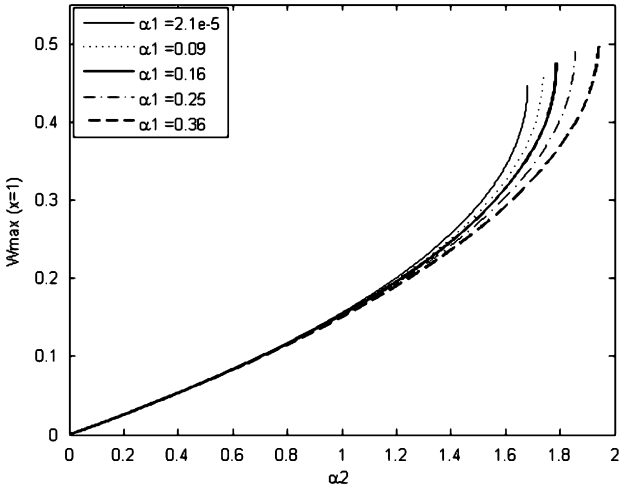

Fig. 4. Variations of the non-dimensional tip deflection w_{max} with α_2 for various values of α_1.

Table 1
Comparison of the static pull-in parameters obtained using the parallel plate capacitance (PPC) model and the second order correction (SOC) of the electrostatic forces.

α_1	$(\alpha_2)_{SPI}$		$(w)_{SPI}$	
	SOC	PPC	SOC	PPC
2.1e–5	1.681	1.681	0.4462	0.4455
0.04	1.706	1.693	0.4530	0.4585
0.09	1.739	1.708	0.4603	0.4584
0.16	1.788	1.728	0.4760	0.4710
0.25	1.854	1.751	0.4894	0.4672
0.36	1.943	1.783	0.5008	0.4728

that geometric nonlinearity has got a stiffening effect on the system and is obvious from Eq. (10). However, the effect of geometric nonlinearity is predicted to be significant for α_1 values 0.09 and above. It has been predicted in the earlier works [10,14,23] that the pull-in instability develops at the normalized maximum deflection (w_{max}) value of 0.33, but the results in Figs. 2–4 show that the non-dimensional static pull-in deflection lies in the range of 0.45 to 0.5. These results indicate that linear theories grossly underestimate the stability limits of the microcantilever. The static pull-in parameters are also compared with the results obtained by neglecting the second term on the right hand side of Eq. (10a), and thus assuming PPC. As shown in Table 1, for values of α_1 equal to 0.09 and above, significant improvement is observed in the static pull-in electrostatic strength $[(\alpha_2)_{SPI}]$ and static pull-in deflection $[(w)_{SPI}]$ parameters when SOC of electrostatic forces is taken into account over PPC approximation. The PPC approximation that neglects the higher order terms is found to underestimate the pull-in parameters.

5.2. Simulation of static behaviour

To derive the discretized static equations, $\sigma_i(t)$ is let independent of time and once all time derivatives in Eq. (13) are set equal to zero, a set of nonlinear algebraic equations is obtained. First the set of nonlinear algebraic equations is numerically solved for a particular number of modes. This is also known as ROM analysis. The microcantilever static deflection is thereafter obtained from Eq. (11) for any DC voltage V. Fig. 5 compares the static solution obtained by directly solving the BVP with the static deflection results of the ROM

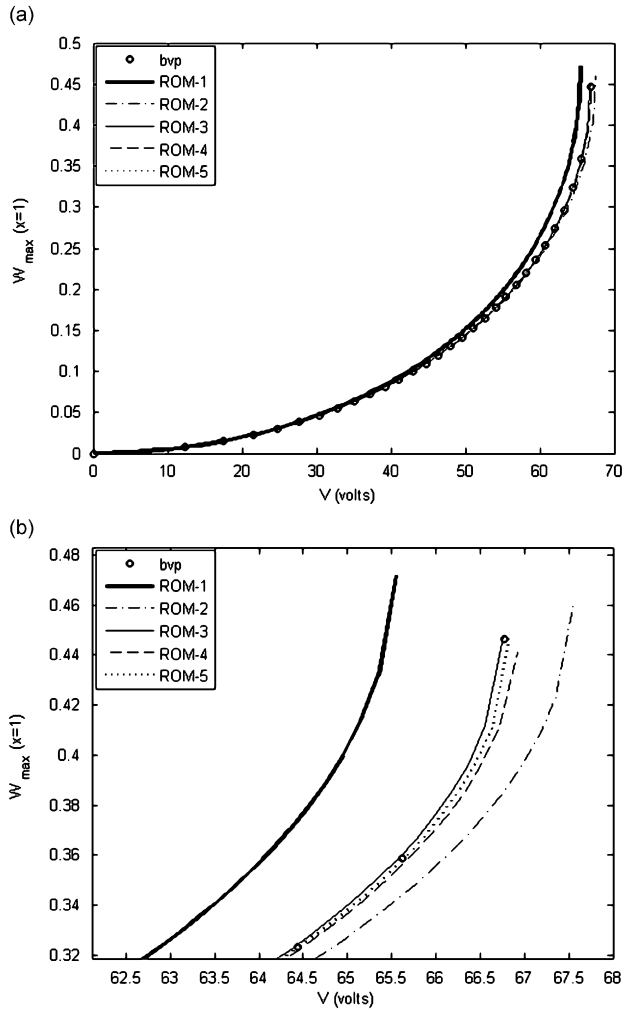

Fig. 5. (a) Predictions of the normalized tip deflection by the ROM of different orders and (b) enlarged plot of the predictions near the pull-in.

simulations. The number of modes is varied from one to five. The design specifications used are same as in Fig. 2. Using different number of modes in the discretization procedure, the predicted values of the V_{SPI} have been plotted in Fig. 6. The results obtained in Ref. [26] shows poor convergence for even number of modes while the results have been published only for odd number of modes in Refs. [27,28]. In the present study, it has been observed (Fig. 5b) that the deflection curve obtained through ROM simulation shifts on either side of the BVP solution, depending on the number of modes considered. The same phenomenon has been also observed and cited in Ref. [47]. It is further noted from Fig. 6 that the results exhibit good convergence when five or more number of modes is taken in the analysis irrespective of the number being even or odd. Convergence is also exhibited with five modes for higher values of α_1. It is therefore recommended that at least five modes should be taken to obtain converged results.

5.3. Simulation of dynamic behaviour

The five-mode ROM has been used, in this section, to study the behaviour of the microcantilever under a suddenly applied DC voltage. A set of nonlinear ODEs obtained from Eq. (13) with $N = 5$ is numerically solved for zero initial conditions to predict the transient behaviour. The dynamic model has been validated by

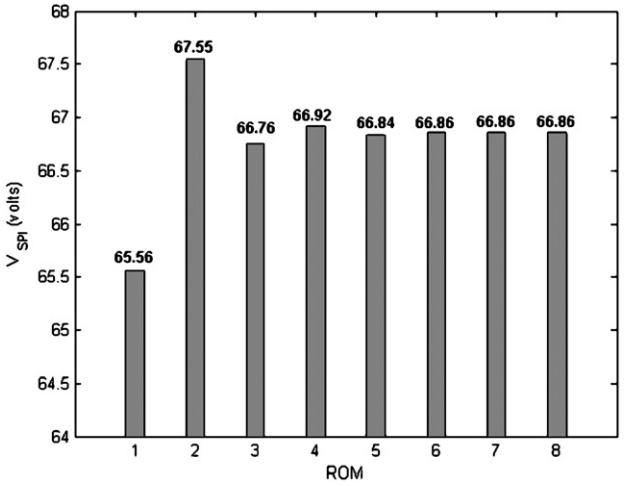

Fig. 6. Comparison of the static pull-in voltages (V_{SPI}) predicted by the ROM of different orders.

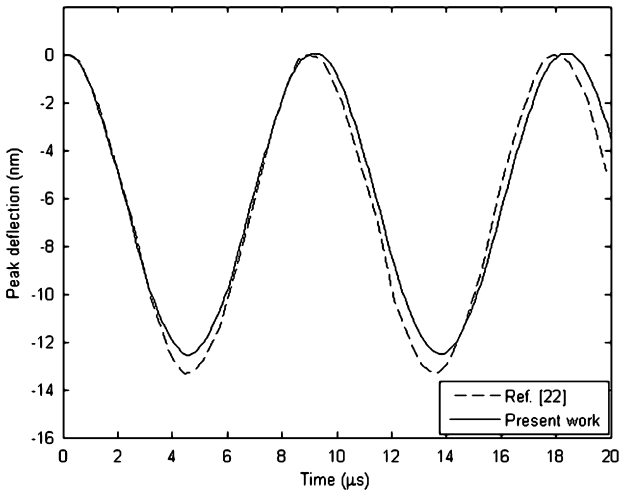

Fig. 7. Non-pull-in response at an applied step voltage of 0.5 V for the beam properties $E' = 169e9\,\text{Pa}$, $b = 10e-6\,\text{m}$, $h = 0.5e-6\,\text{m}$, $d_0 = 0.7e-6\,\text{m}$, $l = 80e-6\,\text{m}$, $v = 0.3$, $\rho = 2231\,\text{kg m}^{-3}$ as used in Ref. [22].

comparing the non-pull-in and pull-in results with the numerical results obtained in Ref. [22]. A step voltage of 0.5 V is applied and the corresponding response of the tip of the microcantilever is plotted as shown in Fig. 7. In the same plot, numerical results obtained in Ref. [22] are also shown. It has been observed that both the results are in excellent agreement. The resonant frequency at 0.5 V is found from the time period as 108.5 kHz compared to 109 kHz as obtained in Ref. [22]. It has been further shown in Fig. 8 that the dynamic pull-in characteristics of the cantilever beam observed at dynamic pull-in voltage (V_{DPI}) of 2.12 V in Ref. [22] match well with the pull-in characteristics at V_{DPI} of 2.25 V obtained with the present numerical scheme. A small deviation in the response characteristics is observed (Fig. 8) after the beam reaches the dynamic pull-in deflection (about 0.44 μm) due to the extreme sensitivity of the response to the actuation voltage at pull-in.

For a particular value of α_1 and varying excitation voltages, the tip deflection time history, as obtained in Fig. 9, predicts periodic motion below a certain critical value of the voltage known as the dynamic pull-in voltage (V_{DPI}). With the time period increasing with voltage, a definite softening effect of the electrostatic forces and the inertial nonlinearity is concluded. For a certain voltage above the critical value, the periodic

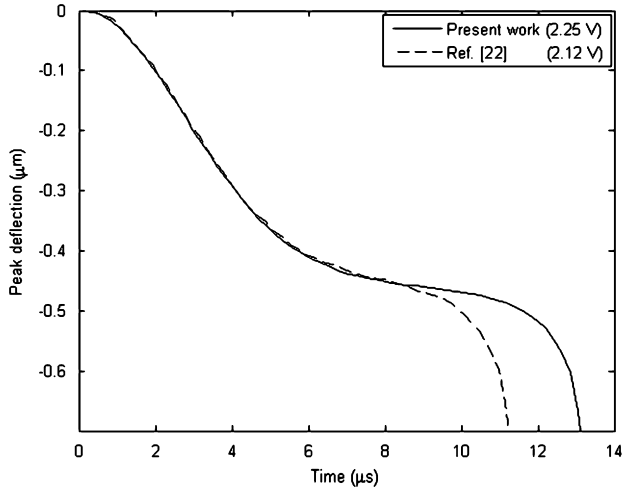

Fig. 8. Pull-in response under step voltage actuations for the beam properties as used in Ref. [22].

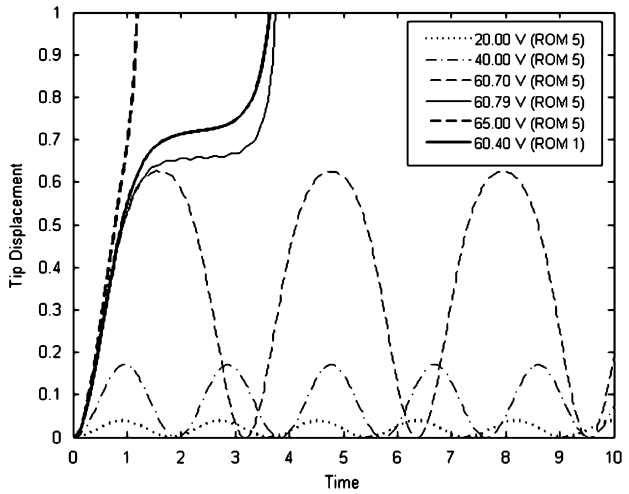

Fig. 9. Deflection time history under various suddenly applied DC voltages for $\alpha_1 = 2.1e-5$.

motion gives away to a divergent motion and the beam abruptly collapses onto the electrode. The quantitative estimation of the dynamic pull-in parameters can be made from the corresponding phase plots as shown in Fig. 10. The dynamic pull-in condition is marked by the separatrix on the phase plane. The dynamic pull-in of the microbeam occurs at an applied voltage (V_{DPI}) of 60.79 V, which is well below the static pull-in voltage (V_{SPI}) of 66.78 V. The dynamic pull-in deflection (0.6–0.7), however, increases thus increasing the travel range of the beam under applied voltages varying as non-smooth function of time. In order to highlight the effect of higher mode, the dynamic pull-in condition for the single mode model (dark continuous line) is also included in Figs. 9 and 10 which clearly show that single-mode model predictions vary significantly from the five-mode model results, for example, the dynamic pull-in of the microbeam is obtained at an applied voltage of 60.40 V with single mode analysis whereas the phenomenon is not observed for five mode analysis carried out at the same (60.40 V) voltage. Ripples can be observed in the response curves for the five mode analysis due to the excitation of higher modes [27].

The effect of geometric nonlinearity on the transient behaviour has been studied in detail. The dynamic pull-in behaviour of beams for various values of α_1 has been simulated. For brevity, simulations for few values of α_1 have been presented in Figs. 11 and 12. Fig. 11 reveals that the electrostatic force for the dynamic pull-in, represented by $(\alpha_2)_{DPI}$, increases significantly with α_1. However, as predicted in the case of static analysis, the

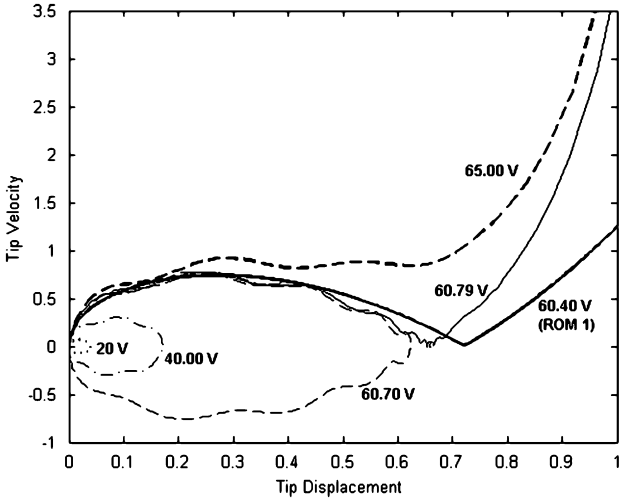

Fig. 10. Phase plot of the five-mode model of the microcantilever excited by various suddenly applied DC voltages, $\alpha_1 = 2.1e-5$.

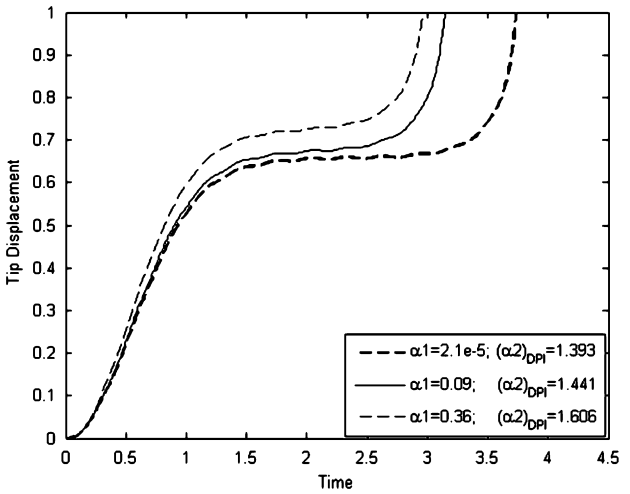

Fig. 11. Deflection time history at pull-in for various values of α_1.

effect of geometric nonlinearity is found to be significant for α_1 values 0.09 and above. From the corresponding phase plot, as shown in Fig. 12, it is observed that before the beam deflection reaches the value of dynamic pull-in deflection (0.6–0.75), the tip velocity at a certain tip displacement is higher for a higher value of α_1, and, is lower for a higher value of α_1 as the beam deflects beyond and approaches the ground electrode. This may be attributed to the fact that for beams with higher values of α_1, $(\alpha_2)_{DPI}$ values are higher resulting in higher beam velocities and larger softening effects whereas the stiffening effects of geometric nonlinearity are larger in the large deflection range. Thus, the overall effect, in the entire deflection range, due to the nonlinearities may be stiffening/softening depending on the relative strengths of the nonlinearities. Moreover, these variations in the tip velocity affect the total time (pull-in time) the beam takes to collapse (represented by non-dimensional tip deflection of unity) onto the electrode as shown in Fig. 11. To highlight the importance of inclusion of higher order corrections in the electrostatic model, a comparison of the dynamic pull-in electrostatic strength $[(\alpha_2)_{DPI}]$ obtained with the SOC model and the PPC model is shown in Table 2. As observed in the static analysis, significant improvement in the dynamic pull-in parameter is obtained with the SOC model for α_1 values equal to 0.09 and above.

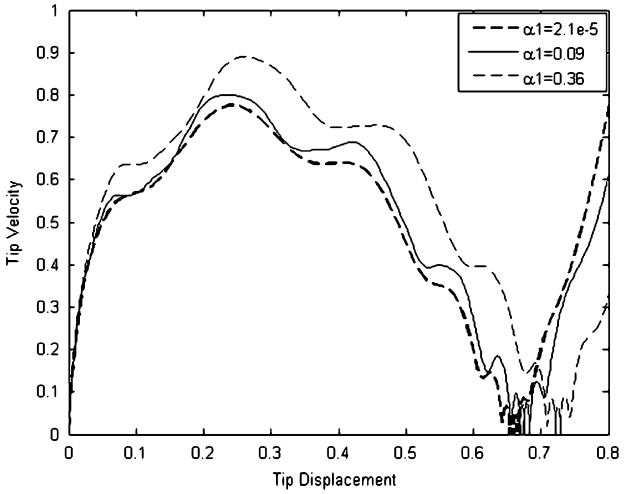

Fig. 12. Phase plot at pull-in for various values of α_1.

Table 2
Comparison of the dynamic pull-in electrostatic strength ($(\alpha_2)_{DPI}$) obtained using the parallel plate capacitance (PPC) model and the second order correction (SOC) of the electrostatic forces.

α_1	$(\alpha_2)_{DPI}$	
	SOC	PPC
2.1e–5	1.393	1.393
0.04	1.414	1.404
0.09	1.441	1.416
0.16	1.480	1.434
0.25	1.534	1.457
0.36	1.606	1.485

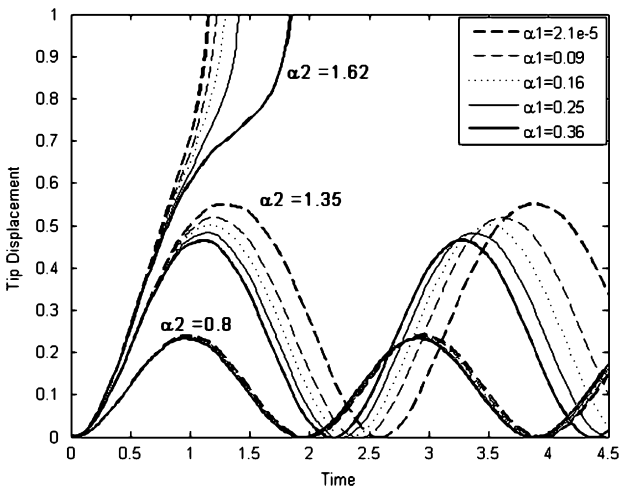

Fig. 13. Deflection time history of the microcantilever at representative values of α_2 in the vicinity and well below pull-in for various values of α_1.

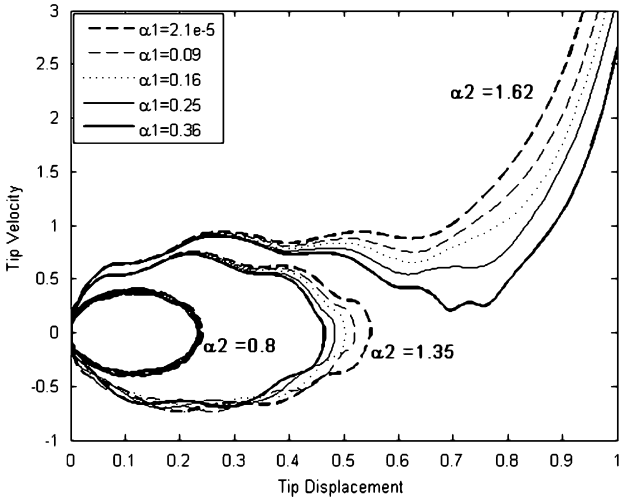

Fig. 14. Phase plot at representative values of α_2 in the vicinity and well below pull-in for various values of α_1.

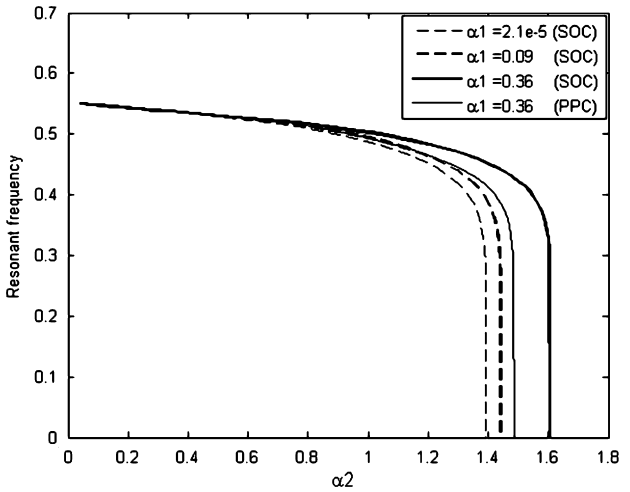

Fig. 15. Variations of the non-dimensional resonant frequency with α_1 for various values of α_2. SOC: second order correction and PPC: parallel plate capacitance.

In order to understand the impact of geometric nonlinearity for actuation voltages in the vicinity and well below pull-in, three practical cases of transient actuation have been presented in Figs. 13 and 14. For each case, the time history and the phase plot have been obtained for beams with various values of α_1 actuated by the electrostatic force of same strength α_2. For the representative case well below pull-in ($\alpha_2 = 0.8$), varying α_1 results in no significant variation in the behaviour, and, as shown in Figs. 13 and 14 the curves overlay each other. In the vicinity of pull-in ($\alpha_2 = 1.35, 1.62$), the overall effects due to the nonlinearities are such that the stiffening effect of geometric nonlinearity is considerable enough. For $\alpha_2 = 1.35$, amplitude (Figs. 13 and 14) and time period (Fig. 13) of the periodic motion decreases with increase in α_1. In the representative case of $\alpha_2 = 1.62$, the pull-in time monotonically decreases with increase in α_1 as shown in Fig. 13. This decreasing trend can be further explained with the help of Fig. 14 which predicts lower tip velocities, almost in the entire deflection range, for beams with higher values of α_1. In Fig. 15, variations of non-dimensional resonant frequency is plotted against α_2 for various values of α_1. The softening effects of the electrostatic forces and the inertial terms are further depicted in the figure. As the applied step voltage increases, the structure is softened

and the resonance reduces. Moreover, for periodic motions well bellow pull-in ($\alpha_2 = 0.8$), varying α_1 results in no significant variation in resonant frequency, whereas, in the vicinity of pull-in the resonant frequency of stable periodic motion increases significantly with increase in α_1. For comparison, resonant frequency plots for various values of α_1 have also been obtained with the PPC approximation and the plot for α_1 value of 0.36 has been shown in Fig. 15. The PPC model predictions of resonant frequencies for higher values of α_2 (>0.8) are found to be significantly underestimated.

6. Conclusions

The static and dynamic behaviour of a microcantilever, with relatively large gap to beam-length ratios, under electrostatic actuation is studied herein with special emphasis on the nonlinear effects due to geometry, electric forces, and inertial terms. The deflections near pull-in being large, model derived on the basis of large deflection assumption effectively predicts the behaviour. In case there is large gap between deformable conductor and ground plane, it is essential to consider higher order corrections of electrostatic forces during the formulation of the model. In the present work, it has been shown that results are much improved when higher order terms are taken into account during static and dynamic analysis. The numerical results of the static analysis are validated with experimental and analytical results available in open literature. According to the results of static analysis where the voltages are applied gradually, a linear model can appreciably predict the static behaviour for small electrostatic forces as the deflections are small. For higher strengths of electrostatic forces close to pull-in, coupled effects of geometric nonlinearity, and nonlinear electrostatic forces with higher order correction terms cause deviation from the linearized results while the effects are significant for initial gap to beam-length ratios of 0.3 and above. Consideration of nonlinearities gives a better estimation of the stability limits which can be advantageously used for design of non-pull-in devices.

A ROM incorporating the correct number of modes provides a compact yet accurate approach to study the behaviour of microstructures. This approach has been extensively evaluated in the present work and has been effectively used to study the transient behaviour of microcantilevers. Results exhibit good convergence for five or more number of modes irrespective of the number being even or odd.

The numerical results of the dynamic analysis are validated with other numerical results available in open literature. According to the results of the transient analysis, nonlinear electrostatic forces and the inertial effects cause softening of the microstructure whereas geometric nonlinearity has got a stiffening effect on the microstructure. The overall effect, in the entire deflection range, due to the nonlinearities may be stiffening/softening depending on the relative strengths of the nonlinearities. At and near pull-in, geometric nonlinearity has got significant effect on the response characteristics for systems with initial gap to beam-length ratios of 0.3 and above. For actuations at applied voltages well below the dynamic pull-in voltage, geometric nonlinearity does not play any significant role. Thus, for applications in and around the pull-in zone, the large deflection model needs to be considered for effective design of microcantilever based microsystems.

References

[1] S. Senturia, *Microsystem Design*, Norwell, Kluwer, MA, 2001.
[2] P. Decuzzi, A. Granaldi, G. Pascazio, Dynamic response of microcantilever-based sensors in a fluidic chamber, *Journal of Applied Physics* 101 (2007) 024303.
[3] J. Teva, G. Abadal, Z.J. Davis, J. Verd, X. Borrisé, A. Boisen, F. Pérez-Murano, N. Barniol, On the electromechanical modeling of a resonating nano-cantilever-based transducer, *Ultramicroscopy* 100 (2004) 225–232.
[4] V. Sazonova, Y. Yaish, H. Ustunel, D. Roundy, T.A. Arias, P.L. McEuen, A tunable carbon nanotube electromechanical oscillator, *Nature* 431 (2004) 284–287.
[5] M. Dequesnes, Z. Tang, N.R. Aluru, Static and dynamic analysis of carbon nanotube-based switches, *Journal of Engineering Materials and Technology* 126 (2004) 230–237.
[6] J.M. Huang, K.M. Liew, C.H. Wong, S. Rajendran, M.J. Tan, A.Q. Liu, Mechanical design and optimization of capacitive micromachined switch, *Sensors and Actuators A* 93 (2001) 273–285.
[7] R. Puers, D. Lapadatu, Electrostatic forces and their effects on capacitive mechanical sensors, *Sensors and Actuators A* 56 (1996) 203–210.
[8] J. Fricke, C. Obermaiar, Cantilever beam accelerometer based on surface micromachining technology, *Journal of Micromechanics and Microengineering* 3 (1993) 100–102.

[9] G.I. Taylor, The coalescence of closely spaced drops when they are at different electric potentials, *Proceedings of Royal Society A* 306 (1968) 423–434.
[10] H.C. Nathanson, W.E. Newell, R.A. Wickstrom, J.R. Davis, The resonant gate transistor, *IEEE Transactions of Electron Devices* ED-14 (3) (1967) 117–133.
[11] B. McCarthy, G.G. Adams, N.E. McGruer, D. Potter, A dynamic model including contact bounce of an electrostatically actuated microswitch, *Journal of Microelectromechanical Systems* 11 (2002) 276–283.
[12] W.C. Xie, H.P. Lee, S.P. Lim, Nonlinear dynamic analysis of MEMS switches by nonlinear modal analysis, *Nonlinear Dynamics* 31 (2003) 243–256.
[13] S. Pamidighantam, R. Puers, K. Baert, H.A.C. Tilmans, Pull-in voltage analysis of electrostatically actuated beam structures with fixed–fixed and fixed-free end conditions, *Journal of Micromechanics and Microengineering* 12 (2002) 458–464.
[14] S. Chowdhury, M. Ahmadi, W.C. Miller, A closed-form model for the pull-in voltage of electrostatically actuated cantilever beams, *Journal of Micromechanics and Microengineering* 15 (2005) 756–763.
[15] S.D. Senturia, R.M. Harris, B.P. Johnson, S. Kim, K. Nabors, M.A. Shulman, J.K. White, A computer-aided design system for microelectromechanical systems (MEMCAD), *Journal of Microelectromechanical Systems* 1 (1992) 3–13.
[16] L.D. Gabbay, J.E. Mehner, S.D. Senturia, Computer-aided generation of nonlinear reduced-order dynamic macromodels I: non-stress-stiffened case, *Journal of Microelectromechanical Systems* 9 (2000) 262–269.
[17] Coventor Inc., Pull-in Voltage Analysis of Electrostatically-Actuated Beams verifying Accuracy of Coventor Behavioural Models 〈http://www.coventor.com/media/fem_comparisons/pullin_voltage.pdf〉.
[18] G. Li, N.R. Aluru, Linear, non-linear and mixed-regime analysis of electrostatic MEMS, *Sensors and Actuators A* 91 (2001) 278–291.
[19] Y.C. Hu, C.M. Chang, S.C. Huang, Some design considerations on the electrostatically actuated microstructures, *Sensors and Actuators A* 112 (2004) 155–161.
[20] E.M. Abdel-Rahman, M.I. Younis, A.H. Nayfeh, Characterization of the mechanical behaviour of an electrically actuated microbeam, *Journal of Micromechanics and Microengineering* 12 (2002) 759–766.
[21] H. Sadeghian, G. Rezazadeh, P.M. Osterberg, Application of the generalized differential quadrature method to the study of pull-in phenomena of MEMS switches, *Journal of Microelectromechanical Systems* 16 (2007) 1334–1340.
[22] S.K. De, N.R. Aluru, Full-Lagrangian schemes for dynamic analysis of electrostatic MEMS, *Journal of Microelectromechanical Systems* 13 (2004) 737–758.
[23] A. Fargas-Marques, J. Casals-Terré, A.M. Shkel, Resonant pull-in condition in parallel-plate electrostatic actuators, *Journal of Microelectromechanical Systems* 16 (2007) 1044–1053.
[24] G.N. Nielson, G. Barbastathis, Dynamic pull-in of parallel-plate and torsional electrostatic MEMS actuators, *Journal of Microelectromechanical Systems* 15 (2006) 811–821.
[25] V. Rochus, D.J. Rixen, J.C. Golinval, Electrostatic coupling of MEMS structures: transient simulations and dynamic pull-in, *Nonlinear Analysis* 63 (2005) e1619–e1633.
[26] M.I. Younis, E.M. Abdel-Rahman, A.H. Nayfeh, A reduced-order model for electrically actuated microbeam-based MEMS, *Journal of Microelectromechanical Systems* 12 (2003) 672–680.
[27] S. Krylov, R. Maimon, Pull-in dynamics of an elastic beam actuated by continuously distributed electrostatic force, *Journal of Vibration and Acoustics* 126 (2004) 332–342.
[28] S. Krylov, Lyapunov exponents as a criterion for the dynamic pull-in instability of electrostatically actuated microstructures, *International Journal of Non-Linear Mechanics* 42 (2007) 626–642.
[29] R.C. Batra, M. Porfiri, D. Spinello, Vibrations and pull-in instabilities of microelectromechanical von Kármán elliptic plates incorporating the Casimir force, *Journal of Sound and Vibration* 315 (2008) 939–960.
[30] R.C. Batra, M. Porfiri, D. Spinello, Vibrations of narrow microbeams predeformed by an electric field, *Journal of Sound and Vibration* 309 (2008) 600–612.
[31] M. Porfiri, Vibrations of parallel arrays of electrostatically actuated microplates, *Journal of Sound and Vibration* 315 (2008) 1071–1085.
[32] P.A. Hassanpour, W.L. Cleghorn, E. Esmailzadeh, J.K. Mills, Vibration analysis of micro-machined beam-type resonators, *Journal of Sound and Vibration* 308 (2007) 287–301.
[33] R.C. Batra, M. Porfiri, D. Spinello, Review of modeling electrostatically actuated microelectromechanical systems, *Smart Materials and Structures* 16 (2007) R23–R31.
[34] S. Krylov, S. Seretensky, Higher order correction of electrostatic pressure and its influence on the pull-in behaviour of microstructures, *Journal of Micromechanics and Microengineering* 16 (2006) 1382–1396.
[35] H. Wagner, Large-amplitude free vibrations of a beam, *Journal of Applied Mechanics* 32 (1965) 887–892.
[36] J. Liua, D.T. Martin, K. Kadirvel, T. Nishida, L. Cattafesta, M. Sheplak, B.P. Mann, Nonlinear model and system identification of a capacitive dual-backplate MEMS microphone, *Journal of Sound and Vibration* 309 (2008) 276–292.
[37] S.R. Hsieh, S.W. Shaw, C. Pierre, Normal modes for large amplitude vibration of a cantilever beam, *International Journal of Solids and Structures* 31 (1994) 1981–2014.
[38] S.N. Mahmoodi, N. Jalili, Non-linear vibrations and frequency response analysis of piezoelectrically driven microcantilevers, *International Journal of Nonlinear Mechanics* 42 (2007) 577–587.
[39] D.H. Hodges, Proper definition of curvature in nonlinear beam kinematics, *American Institute of Aeronautics and Astronautics Journal* 22 (1984) 1825–1827.
[40] A.H. Nayfeh, C. Chin, S.A. Nayfeh, Nonlinear normal modes of a cantilever beam, *Journal of Vibration and Acoustics* 117 (1995) 477–481.

[41] R.C. Batra, M. Porfiri, D. Spinello, Reduced-order models for microelectromechanical rectangular and circular plates incorporating the Casimir force, *International Journal of Solids and Structures* 45 (2008) 3558–3583.
[42] P.M. Osterberg, Electrostatically Actuated Microelectromechanical Test Structures for Material Property Measurements, Ph.D. Thesis, Massachusetts Institute of Technology, 1995.
[43] J.M. Rabaey, *Digital Integrated Circuits*, Prentice-Hall, Englewood Cliffs, NJ, 1996, pp. 438–445.
[44] R.C. Batra, M. Porfiri, D. Spinello, Electromechanical model of electrically actuated narrow microbeams, *Journal of Microelectromechanical Systems* 15 (2006) 1175–1189.
[45] J.A. Pelesko, D.H. Bernstein, *Modeling MEMS and NEMS*, Chapman&Hall/CRC Press, London/New York/Washington, DC, 2003 (Chapter 7).
[46] L.F. Shampine, M.W. Reichelt, J. Kierzenka, Solving boundary value problems for ordinary differential equations in MATLAB with bvp4 〈http://www.mathworks.com〉.
[47] G. Pohit, A.K. Mallik, C. Venkatesan, Free out of plane vibration of a rotating beam with nonlinear elastomeric constraints, *Journal of Sound and Vibration* 220 (1999) 1–25.